Journal of Cluster Science
https://doi.org/10.1007/s10876-020-01791-x

ORIGINAL PAPER

Controlling Metal-Organic Structure by Tuning Molecular Size, Supported Substrate, and Type of Metal

Chenyang Yuan[1] · Na Xue[2] · Yajie Zhang[1] · Na Li[1] · Ziyong Shen[1] · Shimin Hou[1] · Yongfeng Wang[1,3]

Received: 19 February 2020

Abstract
Metal-organic structures are controllably prepared by tuning molecular size, supported substrates, and different kinds of metals. They are characterized by ultra-high vacuum low-temperature scanning tunnelling microscopy and Density functional theory calculations. The relatively larger size of all-trans-retinoic acid (ReA) compared to (2E,4E)-3-methyl-5-(2,6,6-trimethylcyclohex-1-enyl)penta-2,4-dienoic acid (DiA) leads to a bigger gap between neighboring ReA in a tetramer and allows for insertion of molecules, forming high density patterns. ReA forms various structures with different ratios (4:0, 3:1, 2:2) of the two chiral enantiomers on the less reactive Au(111) other than Ag(111). Unlike transition metals, electrostatic attraction between molecules and alkali metals is the origin of the formation of large quartet islands.

Keywords STM · Self-assembly · Metal-organic structure · Chirality coordination · Substrate effect

Introduction

Designing and constructing metal-organic structures, including one-dimensional polymers, two-dimensional networks and three-dimensional frameworks [1–5], have attracted lots of interest recently. The reaction conditions can be adjusted to get products of certain structures. The molecular adsorption chirality helps to generate more interesting and useful structures. So research about the chiral behaviour in the formation of metal-organic structures is an urgent task [6]. Molecular size and substrate also have impacts on the metal-organic frameworks (MOFs) [7]. The molecular size directly affects the assembly patterns while the molecule-substrate interaction may influence the diffusion of molecules. Most previous research mainly focuses on transition metals, like Fe [8–11], Co [12–14], Ni [15, 16]. However, Alkali metals also have significance in many fields, such as Na and K are electrolytes in living organisms and have important biological functions. Therefore MOFs consisting alkali metals are worth of serious investigations.

In this work, we use all-trans-retinoic acid (ReA) and (2E,4E)-3-methyl-5-(2,6,6-trimethylcyclohex-1-enyl) penta-2,4-dienoic acid (DiA), two molecules of very similar configurations but different lengths, expecting to have a variety of assembly networks through coordination with metal atoms. Fe and Na are compared in this research to illustrate how the transition metals and alkali metals interact with organic molecules. The influence of the supported substrate on the metal-organic structures is also investigated.

Materials and Methods

The experiment is performed with an ultrahigh vacuum low-temperature STM (Unisoku 1500) at 4.9K. The Au(111) and Ag(111) surface are argon-ion sputtered and annealed for several cycles. The cut Pt/Ir tip is annealed in

✉ Shimin Hou
smhou@pku.edu.cn

✉ Yongfeng Wang
yongfengwang@pku.edu.cn

[1] Key Laboratory for the Physics and Chemistry of Nanodevices, Department of Electronics, Peking University, Beijing 100871, China

[2] Peking University Information Technology (Tianjin, Binhai), Tianjin 300450, China

[3] Beijing Academy of Quantum Information Sciences, West Bld.#3, No.10 Xibeiwang East Rd, Haidian District, Beijing 100193, China

Published online: 03 April 2020

vacuum first and then dipped onto the metal substrate in a controlled manner to obtain high quality STM images. All STM images are obtained and processed with WSxM.

Density Functional Theory (DFT) calculations are performed using a plane wave basis set and the projector augmented wave method [17]. The exchange and correlation energy is treated with the Perdew-Burke-Ernzerhof (PBE) form of the generalized gradient approximation [18]. The Van der Waals interaction is included using optB86-vdW dispersion corrected methods. All structures are relaxed until the forces became smaller than 0.03 eV/Å.

Results and Discussion

While achiral molecules were deposited onto metal surface, the molecules became chiral. The enantiomeric forms of the both molecules used in the experiment are presented in the Fig. 1, denoted as L and R, respectively.

The DiA molecules constructed into dimer islands on Ag(111) via hydrogen bonds between two molecules in research before [19]. As for metal coordination, we can find some difference. While co-deposited the DiA molecules and iron atoms, ordered array consisting of tetramers appeared. The STM images and the structure of the tetramers have been illustrated in Fig. 2b, c. The molecules in the tetramers adopted two kinds of chirality. The proportion of the both chirality were the same. The angle between two neighboring molecules is 60 degree, which matches the hexadecimal symmetry of substrate.

The formation of the ordered array is considered to be the result of the van der Waals force between the tetramers. And more interestingly, we find that the tetramers in the array adopted three orientations. We use the black, yellow and blue rhomboids to represent the three orientations. The open structure of the tetramers enables them to interlock with each other but the gaps between them are not big enough for two molecules to insert. So that we can find the ordered holes in the array.

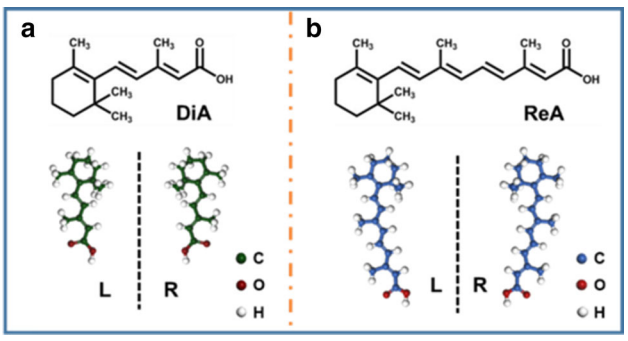

Fig. 1 **a** Schematics and calculated structure of DiA, **b** Schematics and calculated structure of ReA. The enantiomeric forms of the two molecules, denoted as L and R respectively

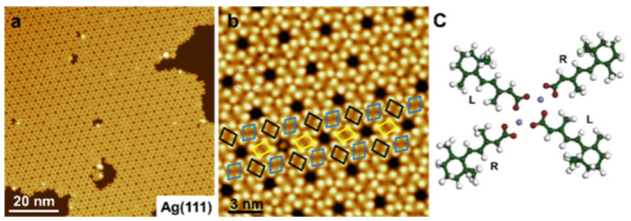

Fig. 2 **a** STM images of dense patterns observed on Ag(111). **b** Trirhomboid ordered array comprising DiA tetramers. The colours used here indicate different orientation (**c**). The calculated molecular structure of a tetramer and the chirality are also represented in the models. Imaging parameters: V_s = 1 V, I_t = 41 pA

To investigate the effect of the molecular size on the formation of coordination structures, we use the longer molecule ReA to deposit with iron on Ag(111). We find that big islands consisting of tetramers dominated on the surface. Differently with the structure for DiA, the molecules in tetramers were all achiral. The STM images and the calculated molecular structures of the tetramers are presented in the Fig. 3. The blue patterns in the Fig. 3b indicates the chirality of the molecules in the tetramers. According to the results above, we can infer that the larger size of molecules caused the bigger gap in the open structures so that the other molecules can insert easily and forms the more close-packed patterns.

The adsorption and coordination structure of molecules are the result of the balance between the molecule–metal-molecular force and the molecule-substrate interaction. In order to have a deeper understanding of the role that the substrate play in this process, we repeat the experiment in less reactive Au(111) metal surface, keeping the other conditions unchanged. While deposited onto the substrate with the iron, a large amount of tetramers islands appeared on the surface. Homochirality and heterochirality are both observed (Fig. 4a), different from the tetramers observed on Ag(111). There are three types of configurations, denoted as α, β, γ. In the configuration α, the four molecules are homochirality, the same as the tetramers on

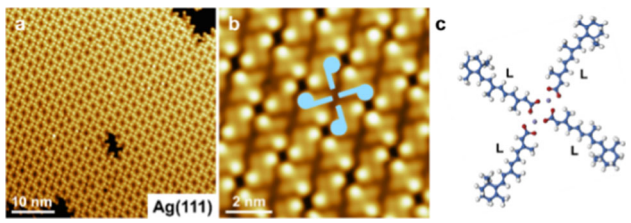

Fig. 3 **a** STM image of the dense pattern observed for Fe and ReA on Ag(111). **b** Magnified image of (**a**) consisting of ReA tetramers. The blue pattern represents a building unit. **c** Optimized molecular structure of the tetramers in (**b**). Imaging parameters: **a** V_s = 500 mV, I_t = 40 pA; **b** V_s = 100 mV, I_t = 40 pA

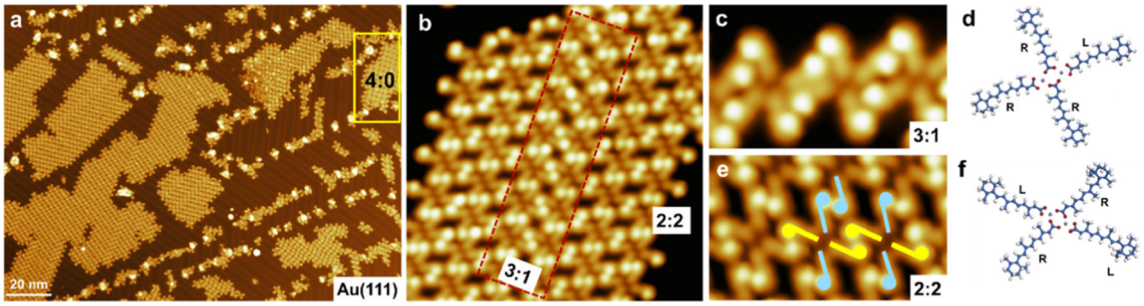

Fig. 4 **a** STM image of the surface after co-deposition of ReA and Fe on Au(111). The yellow square indicates an island of configuration α. **b** Close-up STM image of an island consisting configuration β and γ. **c**, **d** STM image and calculated structure of configuration β. **e**, **f** STM image and calculated structure of configuration γ. Imaging parameters: **a** V_s = 1 V, I_t = 33 pA; **b** V_s = 100 mV, I_t = 43 pA; **c** V_s = 30 mV, I_t = 33 pA; **e** V_s = 60 mV, I_t = 53 pA

Ag(111). In the configurations β, one molecules adopted the reversed chiral conformation of the other three. The ration of the two enantiomeric forms are 2:2 in configuration γ. From the Fig. 4b, the domain areas consisting of configuration β usually lies between two domain areas consisting of configuration γ. The STM images and molecular structures of configuration β and γ are also illustrated in Fig. 4c–f. Highly ordered array comprising the tetramers of configuration γ are observed on the surface. Differently from the ordered arrays of DiA (Fig. 2b), there is enough gap between the two neighbouring molecules in the tetramers here, so two molecules nearby can easily insert in and assemble into high-density pattern. The tetramers interact with each other via Van der Waals force. The difference between the assembly structures on Ag(111) and Au(111) is ascribed to the complicate reconstruction of Au(111). The herringbone reconstruction of Au(111) makes it difficult for molecular diffusion between fcc and hcp regions. Thereafter, heterochiral molecular clusters and small domains are predominantly observed in STM images. In contrast, ReA molecules diffuse more freely on Ag(111) and form large-area ordered islands.

To explore the impacts of different metals, we use Co to replace Fe, and obtain similar results. There have been a big amount of research about the coordination of organic molecules and transition metals, but not much for alkali metals. Having that in mind, we repeat the experiment whether Na interacts with the dehydrogenated with Na in replace of Fe and large quartet islands are experimentally observed (Fig. 5a). According to previous research, ReA molecules only assemble into large islands comprising pentamers or dimers via hydrogen bonds [20, 21]. So the formation of the tetramer superstructure here must be associated with the deposition of Na atoms. As a very active metal, a Na atom easily loses an electron upon deposition on the surface. In this situation, the property of a deposited Na atom is close to that of a Na^+ ion. To find out carboxyl group, we deposit ReA and NaCl on Au(111)

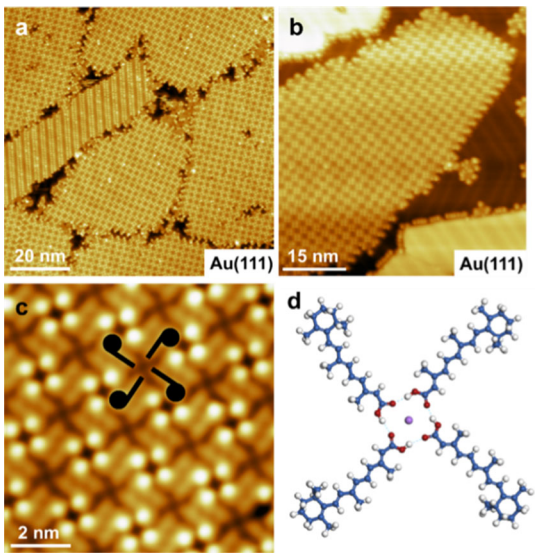

Fig. 5 **a** STM image of quartet island of Na and ReA on Au(111). **b** STM image of large quartet islands after co-deposition of NaCl and ReA onto Au(111). **c** Close-up image of the tetramers shown in (**b**). **d** Structure of a unit consisting four ReA and a Na atom. The electrostatic attraction between Na and O is the cause of this structure

again. Interestingly, large ordered islands of tetramers also appeared, as shown in Fig. 5b, c. The Na^+ may diffuse from the boundary of the NaCl islands and 'dissolve' into the islands of ReA molecules. Due to electrostatic repulsion between Na^+, there must be only one Na^+ in the center of the tetramers. As Na^+ is inert, the carboxyl group in the tetramer should not be dehydrogenated. From these results, we can conclude that the formation of the tetramer by ReA and Na must be mainly due to the electrostatic attraction between O and Na ions, as the optimized structure shown in Fig. 5d. Meanwhile, hydrogen bonds between ReA help to improve the stability of structures.

In summary, we have successfully prepared several metal-organic structures by tuning molecular size, supported substrates, and different kinds of metals. For smaller DiA molecules, the molecule–substrate interaction leads to

the formation of hexagonal Fe-coordinated patterns. The intermolecular interaction between larger ReA molecules changes the coordinated pattern to be nearly four-fold symmetric. Different to the reconstructed Au(111), large-scale molecular arrays can be prepared on Ag(111) because molecules can diffuse more freely on the substrate. Unlike the coordination interaction between Fe and O, electrostatic attraction between O and Na ions makes the most contribution for the formation of tetramers by Na and ReA molecules. This work will be of significance for controllable preparation of metal-organic structures on surface.

Acknowledgements This work is supported by the Ministry of Science and Technology (2018YFA0306003,2017YFA0205003), National Natural Science Foundation of China (21972002,21902003) and China Postdoctoral Science Foundation (CPSF) (2019T120010, 2019M660296). DFT calculations are carried out on TianHe-1A at National Supercomputer Center in Tianjin and supported by High-performance Computing Platform of Peking University.

Compliance with ethical standards

Conflict of interest The authors declare that they have no conflict of interest.

References

1. P. García-García, M. Müller, and A. Corma (2014). *Chem. Sci.* **5**, 2979.
2. B. O. Stefan Leininger and Peter J. Stang (2000). *Chem. Rev.* **100**, 853–908.
3. T. R. Cook, Y. R. Zheng, and P. J. Stang (2013). *Chem. Rev.* **113**, 734–777.
4. B. Moulton and M. J. Zaworotko (2001). *Chem. Rev.* **101**, 1629–1658.
5. M. El Garah, A. Ciesielski, N. Marets, V. Bulach, M. W. Hosseini, and P. Samori (2014). *Chem. Commun.* **50**, 12250–12253.
6. Y.-F. Y. En-Qing Gao, Shi-Qiang Bai, Zheng He, and C.-H. Yan (2004). *J. Am. Chem. Soc.* **126**, 1419–1429.
7. T. Suzuki, T. Lutz, D. Payer, N. Lin, S. L. Tait, G. Costantini, and K. Kern (2009). *Phys. Chem. Chem. Phys.* **11**, 6498–6504.
8. P. Larpent, A. Jouaiti, N. Kyritsakas, and M. W. Hosseini (2019). *Chem. Commun.* **55**, 91–94.
9. P. Knecht, N. Suryadevara, B. Zhang, J. Reichert, M. Ruben, J. V. Barth, S. Klyatskaya, and A. C. Papageorgiou (2018). *Chem. Commun.* **54**, 10072–10075.
10. X. Zhang, N. Li, L. Liu, G. Gu, C. Li, H. Tang, L. Peng, S. Hou, and Y. Wang (2016). *Chem. Commun.* **52**, 10578–10581.
11. T. Lin, G. Kuang, X. S. Shang, P. N. Liu, and N. Lin (2014). *Chem. Commun.* **50**, 15327–15329.
12. T. A. Pham, F. Song, M. N. Alberti, M. T. Nguyen, N. Trapp, C. Thilgen, F. Diederich, and M. Stohr (2015). *Chem. Commun.* **51**, 14473–14476.
13. J. Kuliga, L. Zhang, M. Lepper, D. Lungerich, H. Holzel, N. Jux, H. P. Steinruck, and H. Marbach (2018). *Phys. Chem. Chem. Phys.* **20**, 25062–25068.
14. D. Hotger, M. Etzkorn, C. Morchutt, B. Wurster, J. Dreiser, S. Stepanow, D. Grumelli, R. Gutzler, and K. Kern (2019). *Phys. Chem. Chem. Phys.* **21**, 2587–2594.
15. H. Kong, L. Wang, Q. Tan, C. Zhang, Q. Sun, and W. Xu (2014). *Chem. Commun.* **50**, 3242–3244.
16. C. Wang, Q. Fan, S. Hu, H. Ju, X. Feng, Y. Han, H. Pan, J. Zhu, and J. M. Gottfried (2014). *Chem. Commun.* **50**, 8291–8294.
17. G. Kresse and D. Joubert (1999). *Phys. Rev. B.* **59**, 1758–1776.
18. J. P. Perdew, K. Burke, and M. Ernzerhof (1996). *Phys. Rev. Lett.* **77**, 3865–3869.
19. C. Yuan, N. Xue, X. Zhang, Y. Zhang, N. Li, Q. Xue, T. Wu, S. Hou, and Y. Wang (2019). *Chem. Commun.* **55**, 5427–5430.
20. S. Karan, Y. Wang, R. Robles, N. Lorente, and R. Berndt (2013). *J. Am. Chem. Soc.* **135**, 14004–14007.
21. C. Li, N. Li, L. Liu, Y. Zhang, C. Yuan, L. Peng, S. Hou, and Y. Wang (2017). *Chem. Commun.* **53**, 2252–2255.